REPORT DOCUMENTATION PAGE

Form Approved
OMB No. 0704-0188

PLEASE DO NOT RETURN YOUR FORM TO THE ABOVE ORGANIZATION.

1. REPORT DATE *(DD-MM-YYYY)*	2. REPORT TYPE	3. DATES COVERED *(From - To)*
22 JUNE 2011	FINAL REPORT	01 APR 2007 TO 31 MAR 2011

4. TITLE AND SUBTITLE

DEVELOPMENT OF SILICA FIBERS AND MICROSTRUCTURES WITH LARGE AND THERMODYNAMICALLY STABLE SECOND ORDER NONLINEARITY

5a. CONTRACT NUMBER

FA9550-07-1-0357

5b. GRANT NUMBER

5c. PROGRAM ELEMENT NUMBER

61112F

6. AUTHOR(S)

DR YONG XU

5d. PROJECT NUMBER

2301

5e. TASK NUMBER

AX

5f. WORK UNIT NUMBER

7. PERFORMING ORGANIZATION NAME(S) AND ADDRESS(ES)

VIRGINIA POLYTECHNIC INSTITUTE & S VIRGINIA TECH
1880 PRATT DR STE 2006
BLACKSBURG, VA 24060

8. PERFORMING ORGANIZATION REPORT NUMBER

9. SPONSORING/MONITORING AGENCY NAME(S) AND ADDRESS(ES)

AFOSR/NL
875 NORTH RANDOLPH STREET
SUITE 325, ROOM 3112
ARLINGTON, VA 2203-1768

10. SPONSOR/MONITOR'S ACRONYM(S)

11. SPONSOR/MONITOR'S REPORT NUMBER(S)

AFRL-OSR-VA-TR-2012-0186

12. DISTRIBUTION/AVAILABILITY STATEMENT

APPROVED FOR PUBLIC RELEASE. DISTRIBUTION IS UNLIMITED

13. SUPPLEMENTARY NOTES

14. ABSTRACT

Summary: During the last four years, we have accomplished the following goals.
• We have developed the theoretical framework for the analysis of second-order nonlinearity in the proposed nonlinear fibers and microspheres.
• We have experimentally demonstrated second harmonic generation in the proposed nonlinear fibers and established good agreement between theoretical predictions and experimental measurements.
• We have obtained preliminary results that can achieve intermodal phase matching as well as quasi-phase matching based on plasmonic enhancement.
• We have established that microspheres covered with nonlinear polymers and plasmonic nanoparticles can maintain high Q whispering gallery modes.

15. SUBJECT TERMS

16. SECURITY CLASSIFICATION OF:			17. LIMITATION OF ABSTRACT	18. NUMBER OF PAGES	19a. NAME OF RESPONSIBLE PERSON
a. REPORT	b. ABSTRACT	c. THIS PAGE			DR HOWARD SCHLOSSBERG
					19b. TELEPHONE NUMBER *(Include area code)* 703-696-7549

Reset

Standard Form 298 (Rev. 8/98)
Prescribed by ANSI Std. Z39.18

Development of silica fibers and microstructures with large and thermodynamically stable second order nonlinearity

Dr. Howard Schlossberg (Program Manager), Contract Number: FA9550-07-1-0357

Yong Xu (PI), Virginia Tech

Summary: During the last four years, we have accomplished the following goals.

- We have developed the theoretical framework for the analysis of second-order nonlinearity in the proposed nonlinear fibers and microspheres.
- We have experimentally demonstrated second harmonic generation in the proposed nonlinear fibers and established good agreement between theoretical predictions and experimental measurements.
- We have obtained preliminary results that can achieve intermodal phase matching as well as quasi-phase matching based on plasmonic enhancement.
- We have established that microspheres covered with nonlinear polymers and plasmonic nanoparticles can maintain high Q whispering gallery modes.
- We have published three peer reviewed papers in Applied Physics Letters, Physical Review Letters, and Optics Express. (The optics express paper was selected as the highlighted article of June 2011.) Two additional manuscripts are under preparation. The three published papers are listed below:

  C. Daengngam, M. C. Hofmann, Z. Liu, A. Wang, J. R. Heflin, and Y. Xu, "Demonstration of a cylindrically symmetric second-order nonlinear fiber with self-assembled organic surface layers," *Opt. Express*, **19** (11), 10326-10335 (2011).

  Y. Xu, M. Han, A. Wang, Z. Liu, and J. R. Heflin, "Second order parametric processes in nonlinear silica microspheres," *Phys. Rev. Lett*., **100,** Art#163905, (2008).

  Y. Xu, A. Wang, J. R. Heflin, and Z. Liu, "Proposal and analysis of a silica fiber with large and thermodynamically stable second order nonlinearity." *Appl. Phys. Lett.*, **90** (21), Art # 211110, (2007).

- Two graduate students obtained their Masters' degree through support of this grant. Two additional Ph.D. candidates will defend their Ph.D. based on this project.

1. Introduction

The advance in silica fiber technology has not only revolutionized modern telecommunications but also created major research disciplines such as nonlinear fiber optics. Yet even after decades of development, research in nonlinear fiber optics remains primarily limited to third-order effects such as four-wave-mixing and optical solitons [1]. This fundamental limitation arises from a simple fact: As an amorphous material with full inversion symmetry, silica glass cannot possess second-order nonlinearity. Consequently, until now it has been very difficult to use silica fiber to realize some of the most important second-order processes including second harmonic generation (SHG) and optical parametric oscillation (OPO).

Recently, a few research groups have developed several methods that aim to overcome the lack of second-order nonlinearity in silica fiber devices. Most such methods are based on poling silica glass using external fields, with examples including optical poling [2, 4], electrical poling [5-9], UV poling [10-11], corona poling [12-14], or doping microstructures into fibers [15-17]. However, since all such techniques introduce a preferred direction into silica glass, the induced

second-order nonlinearity is thermodynamically unstable and tends to decay over time [2, 18-20]. In contrast to current methods, here we demonstrated that it is possible to generate significant second-order nonlinearity in a silica fiber by coating it with layers of radially aligned nonlinear molecules [21, 22]. The coating process can be accomplished through a layer-by-layer self-assembly, where the alignment of the nonlinear molecules is maintained through electrostatic interaction. As a result, the second-order nonlinearity of the proposed fibers is thermodynamically stable, which cannot currently be achieved by any other means [23]. Furthermore, the proposed fibers can generate significant second-order nonlinear responses despite their full rotational symmetry. In fact, for such fibers, instead of being a hindrance, the high degree of symmetry directly leads to a symmetry-enforced selection rule that can produce quantum entanglement [21, 22].

This report is organized as follows. In section 2, we describe the process of nonlinear fiber fabrication and characterization. Then in section 3, we report our experimental study on the second harmonic generation (SHG) from such nonlinear fibers. In addition, we also report a detailed comparison between theoretical predictions and experimental results of SHG. In section 4 and 5, we describe the preliminary experimental results on intermodal phase matching and a method that can be used to achieve quasi-phase matching based on plasmonic enhancement. In section 6, we report our studies on how self-assembled nonlinear polymers and plasmonic nanoparticles impact microsphere Q factors. Then, in section 7, we list papers published as well as manuscripts under preparation.

2. Fiber Sample Fabrications

The schematic of the silica-based nonlinear fiber is shown in Fig. 1(a). It consists of a uniform silica core covered by layers of radially aligned nonlinear molecules. The fabrication of such nonlinear fibers begins with pulling silica fiber tapers with diameter in the range of a few microns. (Such a small diameter is necessary in order to achieve strong interaction between the optical field and the nonlinear molecules.) Our taper pulling process is similar to the procedures described in Refs. [24] and [25]. Briefly, we placed a silica fiber between two fiber clamps and used a propane-oxygen flame to heat the fiber. As the glass softens, we slowly pulled the two clamps apart. The pulling speed was precisely controlled by two Newport UTM100CC.1 motion stages, which enabled us to tailor the waist size and the profile of the fiber taper. All fiber tapers in the following discussions were produced using a multimode fiber (50 μm core and 125 μm cladding, Corning ClearCurve OM2), where the taper waist radius ranges from 2.8 to 7.5 μm. Optical transmission of such fiber tapers is typically above 90%.

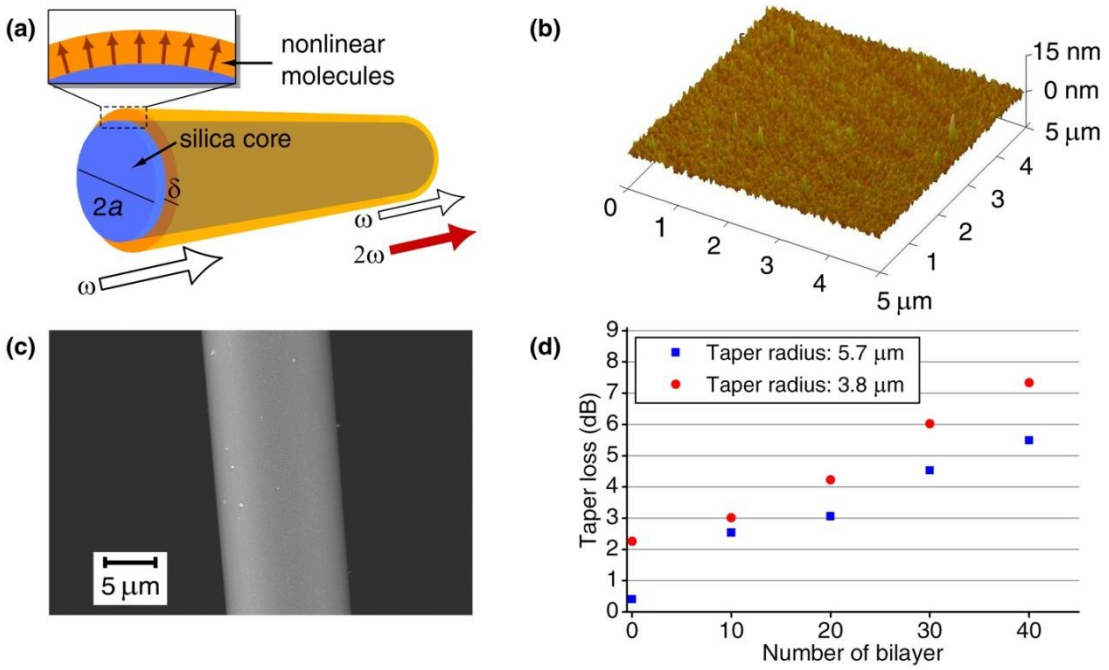

Fig. 1. Nonlinear coating on a silica fiber. (a) The schematic structure of the nonlinear fiber. The radially aligned nonlinear molecules provide a second-order susceptibility tensor dominated by the component. (b) The AFM image of 10-bilayer nonlinear self-assembled film on a planar glass substrate shows highly uniform coating. (c) SEM image of a nonlinear fiber with 10-bilayer coating. (d) The transmission loss of a coated taper at wavelength of 1294 nm was recorded for every 10-bilayer film deposition.

The next step in the nonlinear fiber fabrication is the self-assembly of radially aligned nonlinear molecules. The coating process is based on a novel hybrid covalent/ionic self-assembled multilayer technique developed by Dr. Heflin [23]. Briefly, we dipped the fiber taper into a polycationic solution containing poly(allyamine hydrochloride) (PAH) with pH 7.0 and 10 mM concentration, whereupon a monolayer of positively charged PAH film grew uniformly on the negatively charged taper surface. Following PAH deposition, we dipped the fiber sample into an aqueous solution containing nonlinear molecules Procion Brown MX-GRN (PB) at pH 10.5, 5 mg/mL concentration and 0.5 M NaCl added. At this pH, the dichlorotriazine moieties of PB form covalent bonds with the unprotonated amines of PAH. Upon deposition of the sequential PAH layer at pH 7.0, the negatively-charged sulfonates of PB bind electrostatically with the protonated amine groups of PAH. The deposition of each monolayer requires less than two minutes and can be repeated to produce multilayer nonlinear optical films [26].

The nonlinear optical properties of PAH/PB films on planar glass substrate have been studied. It was found that the second-order nonlinear tensor of the film was dominated by the zzz component with $\chi_{zzz}^{(2)} = 21$ pm/V, approximately two third the value of $LiNbO_3$ [23]. (The z direction is normal to the planar glass substrate.) Since molecular orientation of the PAH/PB film is maintained through electrostatic and covalent interactions, the nonlinear susceptibility of the film is thermodynamically stable. For example, the self-assembled films exhibit excellent thermal and temporal stability with no decrease of $\chi_{zzz}^{(2)}$ after a temperature cycles to 150 ℃ for 24 hours or under ambient condition for more than two years [23]. They are also mechanically stable and impervious to immersion in water and most organic solvents.

Since the thickness of each PAH/PB bilayer is only ~1 nm [23], the nonlinear molecules can conformally coat the silica fiber while maintaining a radial alignment. Fig. 1(b) shows an atomic force microscope (AFM) image of 10-bilayer PAH/PB film on a planar glass substrate. As

revealed by the AFM image, the PAH/PB film is highly uniform, and the standard deviation of film thickness is only 3 nm. Fig. 1(c) shows a scanning electron microscope (SEM) image of a silica fiber taper coated with 10-bilayer PAH/PB film. The SEM image indicates a smooth and uniform nonlinear coating occasionally marred by the presence of dust particles. Since all fiber fabrication was performed outside a clean room, the appearance of dust particles is not unexpected. The transmission loss of the nonlinear fiber taper was monitored throughout the entire self-assembly process. Fig. 1(d) shows the measured transmission loss for two nonlinear fiber samples with different taper radius and numbers of PAH/PB bilayers. We note that even with 40 bilayers of nonlinear film, the transmission loss through the entire taper region is 5-7 dB. The transmission loss can potentially be further lowered by reducing the number of dust particles attached to the fiber taper [27].

3. Second Harmonic Characterization of Nonlinear Fiber Tapers

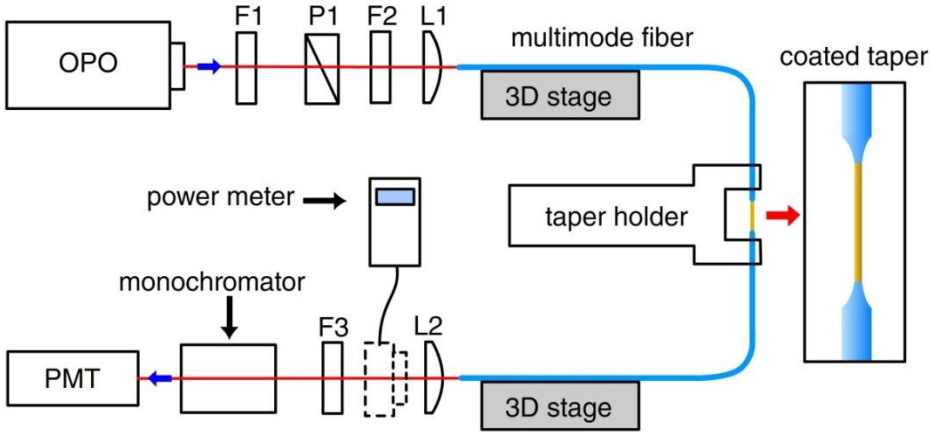

Fig. 2. Schematic diagram of the experimental setup. An infrared, nanosecond-pulsed pump beam obtained from an OPO system is coupled into a multimode fiber. The beam propagates through a nonlinear taper, and interacts with the second-order nonlinear molecules on the taper surface. The output SHG signal is collimated, filtered and finally detected by a PMT.

The nonlinear optical properties of the fiber taper are characterized through second harmonic generation. As shown in Fig. 2, an OPO is used to generate linearly polarized pump pulses at 1294 nm. The pulse width is 10 ns with a repetition rate of 20 Hz. The pump pulse energy is adjusted by rotating the polarizer (P1) and measured using an optical power meter. (The power meter will be removed when we perform SHG measurements.) Two long-pass filters (F1 and F2) are used to remove background second harmonic signals generated by the polarizer and other optical components (e.g., any surface SHG signals). The pump light is coupled into a multimode fiber and transmitted through a nonlinear taper region. The second harmonic signals generated by the nonlinear taper are confined within the silica core and coupled back into the multimode fiber. At the fiber output, both the fundamental pump and the second harmonic signal are collimated back into free space, where we used a short pass filter (F3) to remove the pump light. The wavelength of the second harmonic signal is verified by a monochromator, and its power is detected by a photomultiplier tube (PMT). To eliminate any inconsistency in coupling free space optical signals in and out of the silica fiber, the entire fiber collimation systems, which consists of multiple lenses and translation / rotation stages, are kept unchanged during the measurement processes. Different nonlinear fiber samples are connected with the multimode fiber through fiber splicing. The total splicing loss is consistently kept to be less than 0.01 dB.

Previous work [28, 29] suggests that common silica fibers may exhibit weak second-order nonlinear responses (e.g., SHG and SFG) if pump peak power reaches the level of 100 kW. To

eliminate such effects, we limit the peak power of our pump pulses to 400 W and below, and keep the total length of the multimode fiber to be 2 m or less. Furthermore, we quantify the background SHG signal strength by bypassing the nonlinear taper in Fig. 2 and directly splicing the two sections of multimode fiber together. Under the aforementioned experimental conditions, the background SHG signals of our measurement system cannot be detected. Furthermore, by using a moderate pump power, we can avoid the problem of optically damaging the self-assembled organic film through undesirable effects such as photobleaching at high pump intensity.

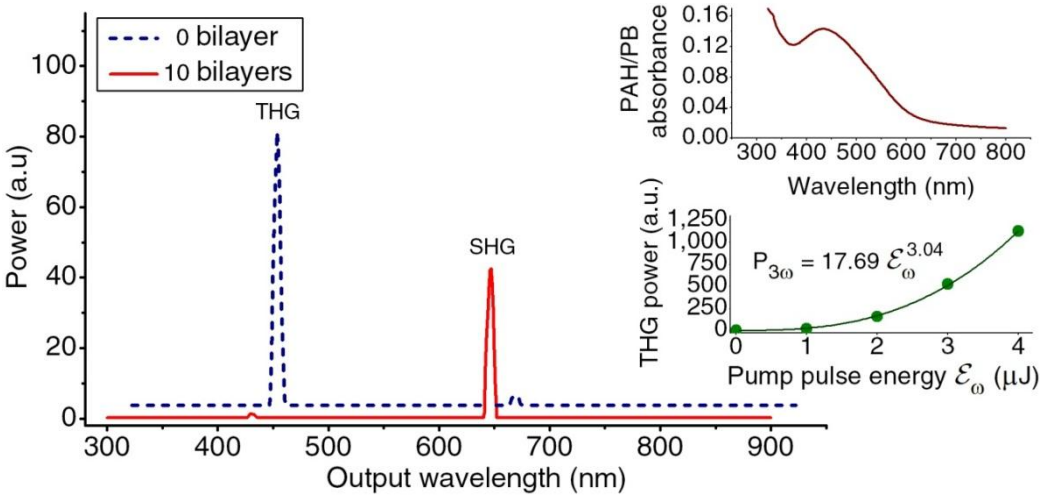

Fig. 3. The THG (at 431 nm) and SHG (at 647 nm) spectra from a bare and a 10-bilayer coated taper, excited by pump pulse energy of 2 μJ at 1294 nm. The bare fiber curve is shifted both vertically and horizontally for clarity. The lower inset confirms a cubic dependency of the THG emitted from the bare taper. With nonlinear coating, we observe an increase in SHG power and decreased THG component due to the film absorption at 431 nm as indicated in the upper inset.

We first verified the existence of SHG by measuring the spectrum of nonlinear optical signal generated by a nonlinear fiber sample. Fig. 3 compares the spectra produced by a fiber taper (waist radius: 3.8 μm) before and after coating with the self-assembled PAH/PB films. For the bare fiber taper (i.e., without nonlinear coating), the measured spectrum clearly contains both a second harmonic component at 647 nm and a third harmonic component at 431 nm. The 431 nm component is due to third harmonic generation (THG) [30, 31], which is further confirmed by the measurement of the THG power as a function of pump pulse energy, as shown in the Fig. 3 inset. The small second harmonic component produced by the bare fiber taper can be attributed to SHG at the air-silica interface in the taper region [32]. After coating the same fiber taper with 10 bilayers of PAH/PB film, we note that the third harmonic signal becomes much weaker. (The reduction in THG power can be attributed to the strong PAH/PB absorption at 431 nm, as indicated in the inset of Fig. 3.) The second harmonic signal produced by the PAB/PB-coated nonlinear fiber, on the other hand, becomes much stronger.

To further clarify the origin of SHG, we measured the dependence of SHG power on pump pulse energy using several nonlinear fiber samples. To remove pump polarization dependence, all pump light is linearly polarized, as indicated by our optical system in Fig. 2. To eliminate variations due to different taper geometries, all nonlinear fiber samples were fabricated from the same bare silica taper used in Fig. 3. Our procedure is as follows: We first performed SHG measurement on the bare silica taper followed by depositing 10 bilayers of PAH/PB film on the bare taper. We then performed the SHG measurement again followed by adding 10 additional bilayers of PAH/PB coating. This SHG measurement / film deposition cycle was repeated until

we reached 40 bilayers of PAH/PB film. As shown in Fig. 4, we notice that second harmonic power increases quadratically as a function of the pump pulse energy, a characteristic feature of SHG. Furthermore, an increase in nonlinear film thickness directly leads to an increase in second harmonic power. For a 40-bilayer coating, we observe a 400-fold increase in SHG power compared to the bare taper case. These results confirm that the measured second harmonic component is indeed generated by the nonlinear PAH/PB coating.

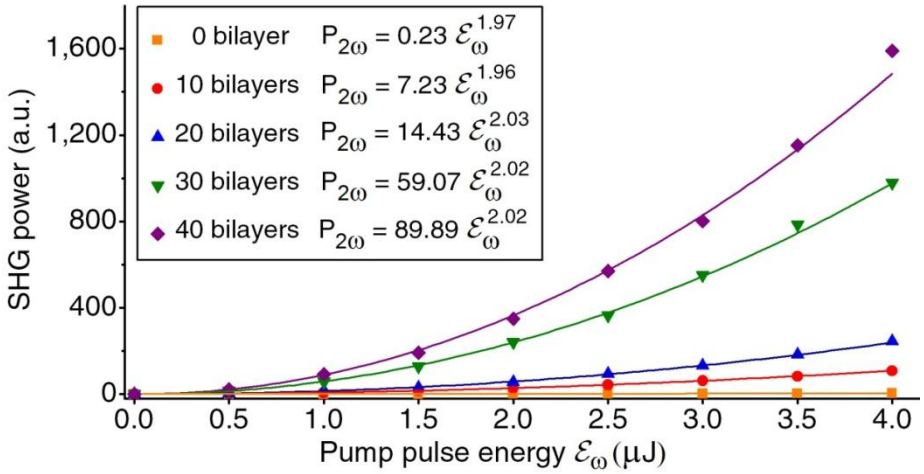

Fig. 4. SHG power as a function of pump pulse energy. The measurement was taken for a 3.8-μm-radius taper with 0, 10, 20, 30 and 40 bilayers of nonlinear film. Each data point is the result of an average of over 100 measurement data and the error bar is smaller than the symbol. The lines are quadratic fits to the data.

The dependence of SHG power with taper waist radius was also studied and the result is shown in Fig. 5. (Refer to next page.) The SHG data was collected from five nonlinear fiber samples with waist radii varying from 2.8 μm to 7.5 μm. All samples are coated with 10-bilayer PAH/PB film, and all SHG measurements are performed using a 1294 nm pump with pulse energy of 2 μJ per pulse (peak power of ~ 200W). The log-log plot for SHG power versus taper radius is shown in Fig. 5 and clearly reveals $1/a^4$ behavior (where a is waist radius), which is consistent with our previous theoretical prediction reported in Ref. [21]:

$$P_{2\omega} = 2\omega^2 \left(\frac{\mu_0}{\varepsilon_r \epsilon_0}\right)^{3/2} \frac{P_\omega^2}{\pi a^2} \left|\frac{\delta}{a}\chi^{(2)}_{zzz}\right|^2 L^2 \times \frac{\sin^2(\Delta\beta L/2)}{(\Delta\beta L/2)^2} \quad (1)$$

In Eq. (1), P_ω is the power of fundamental beam, $P_{2\omega}$ is the power of SHG, ω is the angular frequency of fundamental beam, δ is nonlinear film thickness and L is the taper length (a constant taper waist is assumed). The last term of the equation accounts for phase mismatch between the fundamental and the second harmonic mode, with $\Delta\beta = 2\beta_1 - \beta_2$, where β_1 and β_2 are respectively the propagation constants of fundamental beam and its second harmonic. Eq. (1) predicts a $1/a^4$ power dependence as well as fluctuations due to phase mismatch [i.e, the term]. Both effects are visible from Fig. 5, where we can observe a general trend of $P_{2\omega} \propto 1/a^4$ as well as a small variation around the $1/a^4$ fitting line.

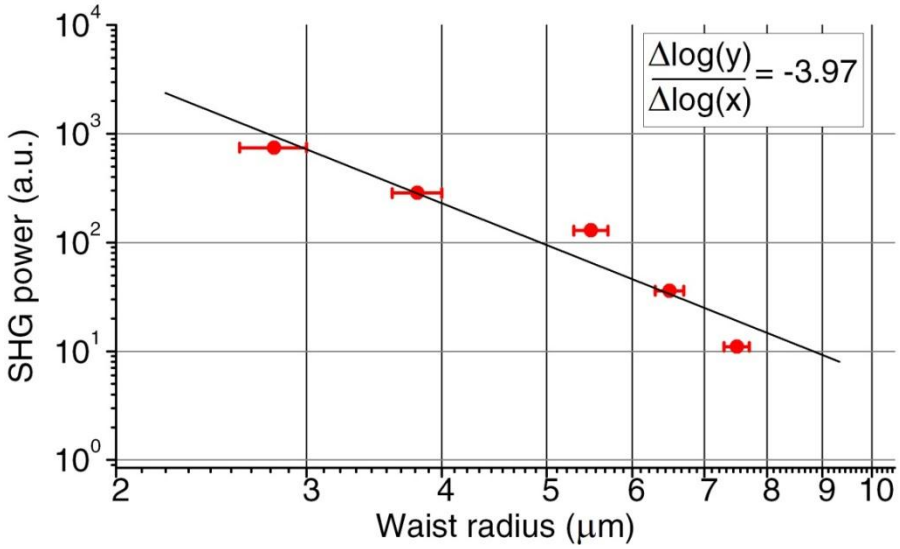

Fig. 5. Dependence of SHG on taper radius. The log-log plot shows the 1/a4 behavior of SHG power with different taper radius. All samples are coated with 10-bilayer films and excited with pulse energy of 2 μJ. The error bars in the x axis indicate the estimated accuracy of taper radii measurements (±0.2 μm) as determined by the optical microscope.

An additional study of the impact of phase mismatch was carried out as follows. To account for the effect of non-uniform taper profile, we follow the procedure in Ref. [21] and obtain a coupled mode equation for SHG in the nonlinear taper:

$$\frac{dE_{2\omega}}{dz} = -i\frac{\omega E_{\omega}^2}{\epsilon_0 v_g}\frac{\delta}{\sqrt{\pi}\epsilon_r^{3/2}a(z)}\chi_{zzz}^{(2)}e^{-i\Delta\beta(z)z} \tag{2}$$

where E_ω and $E_{2\omega}$ are respectively the electric field amplitude of pump and SHG beams, and ug is group velocity at 2ω. (We choose the propagation distance z such that the narrowest fiber taper radius is at z = 0.) In Eq. (2), the only parameter that cannot be readily obtained from experimental conditions is the phase-mismatch term $\Delta\beta = 2\beta_1 - \beta_2$. To calculate this term we assume the fundamental waves are in the HE_{11} mode. This assumption is based on the observation that fiber taper transition is gradual and smooth, which should minimize the excitation of higher order modes such as the HE_{12} mode. This assumption is verified by monitoring the transmission of optical power during the taper pulling process. Fig. 6(a) shows the transmission coefficient as a function of taper pulling time. At the end of taper pulling, the fiber taper radius is approximately 0.5 μm, which is less than the cutoff radius for the HE_{12} mode (0.6 μm at wavelength 980 nm, assuming a fiber with silica core and air cladding). The absence of significant higher order mode coupling is confirmed by the high transmission (T > 90%) throughout the entire taper pulling process.

We can use Eq. (2) to theoretically estimate the efficiency of second harmonic generation. For linearly polarized pump light, the second harmonic mode can be either HE_{21} or TM_{01} mode [21]. In deriving Eq. (2), we have utilized a few simplifying assumptions in Ref. [21] to remove azimuthal dependence. In the final result, i.e., Eq. (2), the choice of either picking HE21 mode or TM_{01} mode only impacts a single parameter: Δβ. For our present study, in which the taper size is several microns, we found that the propagation constants of the HE_{21} and TM_{01} mode are very close. In fact, as shown in Fig. 6(b), the difference between the propagation constant of the HE_{21} and TM_{01} mode is of the order of 10^{-5} or less. Therefore, for the purpose of an order-of-magnitude estimate of second harmonic power, whether we choose HE_{21} or TM_{01} as the second harmonic mode should not make a significant difference.

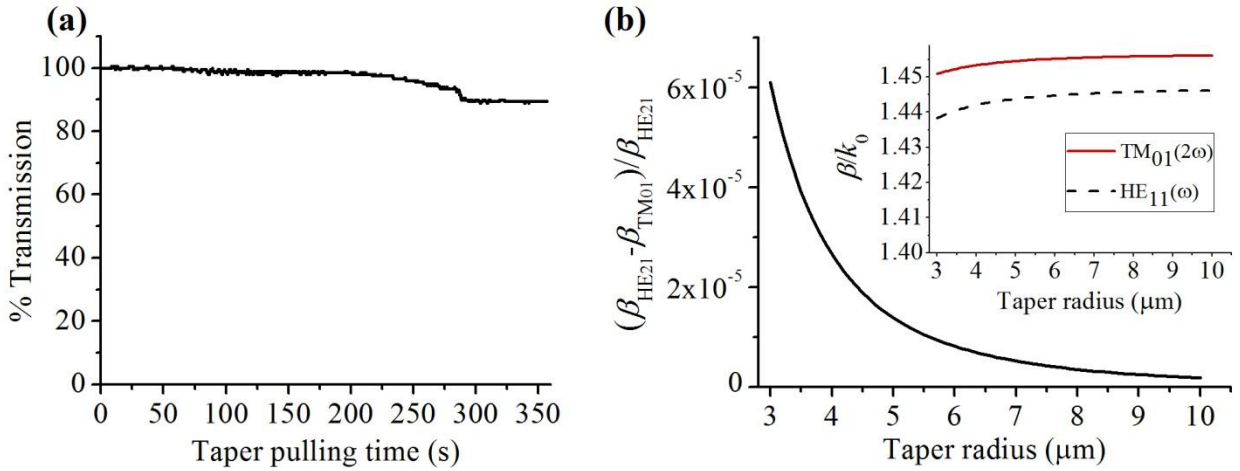

Fig. 6. (a) Typical real-time transmission of optical power (at 980 nm) during the taper pulling process. The taper pulling was stop at the taper radius ~0.5 μm (b) The difference between the propagation constants of the TM_{01} mode and HE21 mode at the SHG wavelength of 647 nm. The inset shows the propagation constant of the TM_{01} (at 647 nm) and HE_{11} mode (at 1294 nm).

We then used an optical microscope to obtain an image of the entire fiber taper region as shown in Fig. 7(a). (Refer to the next page.) Then, using a Matlab program, we converted the microscope image to a binary bitmap, from which we extract fiber radius at any given location. Using this method, we obtained radial profiles of five different fiber tapers. We then compared waist radii obtained using this method with those directly measured from SEM images. For all five samples, the difference between the two approaches is less than 0.2 μm, which is at the resolution limit of an optical microscope.

Following the above assumptions on the propagating modes and using the fiber waist profile extracted from the optical microscope image, we can numerically calculate the value of $\Delta\beta(z)$ as a function of propagation distance z. Once the $\Delta\beta(z)$ is known, we can then numerically integrate Eq. (2) and obtain the power of second harmonic wave. In Fig. 7(b), we perform numerical integration starting from z = -L/2 to z = L/2 with various values of interaction length L, and plot the second harmonic power as a function of the interaction length L. We note that $P_{2\omega}$ in Fig. 6(b) converges to a finite result for L greater than 3000 μm. Therefore, we consider L = 3000 μm to be the effective interaction length that defines the region of strong interaction between nonlinear molecules and the pump field. This observation is also consistent with the taper profile shown in Fig. 7(a), where, at z = ±1500 μm, taper diameter grows to approximately twice of its waist value. The simulation result in Fig. 7(b) also agrees reasonably well with experimental data: For a peak pump power of 400 W at 1294 nm, the numerical integration indicates that we should expect a SHG power of 169.7 μW, whereas the experimentally measured second harmonic peak power is 49.8 μW. The agreement is reasonable, especially considering the fact that the numerical estimate is obtained without using any empirical fitting parameters.

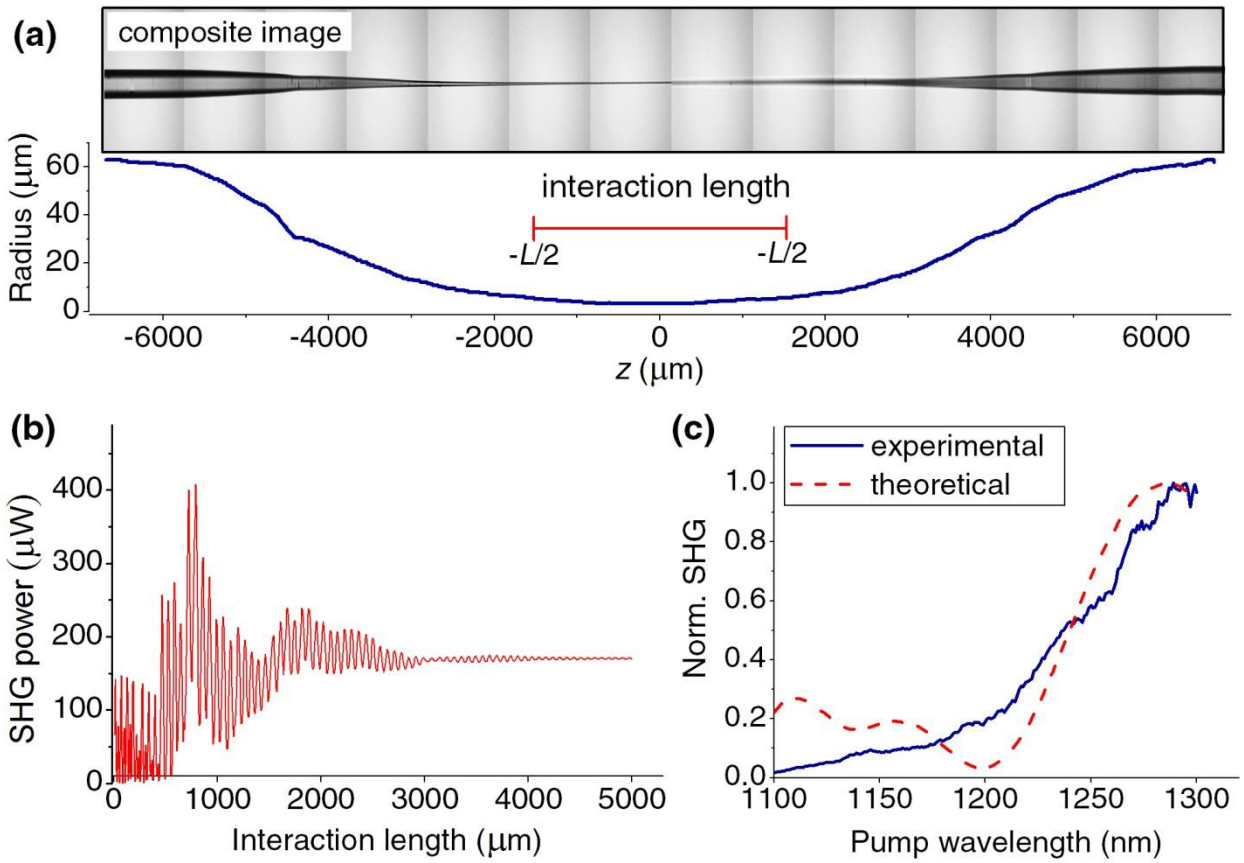

Fig. 7. (a) The profile of a 3.8-μm taper obtained by combining sequential images taken using an optical microscope (Leica DMI-6000 B). (b) Theoretical estimate of SHG power as a function of taper interaction length. The result is obtained by numerically integrating the coupled mode Eq. (2) while using the taper profile determined in (a). (c) Theoretical simulation and experimental result of SHG power versus pump wavelength. Both results are normalized with respect to their corresponding peak SHG power.

By following the procedure outlined above and using parameters extracted from the actual nonlinear fiber, we can also calculate the strength of second harmonic signal generated by the nonlinear fiber as a function of pump wavelength. (The pump peak power is fixed at 400W.) The numerical result is shown in Fig. 6(c) as a dashed line. The corresponding experimental result was obtained by tuning the OPO pump wavelength from 1100 nm to 1300 nm with a wavelength step of 1 nm. The pump power was maintained constant throughout the wavelength scan. At any given pump wavelength, the monochromator is adjusted so that only second harmonic light can pass through and be detected by the PMT. The experimentally measured SHG power is shown in Fig. 7(c) as a solid line. Again, we observe good agreement between the theoretical prediction and the experimental results. The small discrepancy between the theoretical predictions and the experimental results in the shorter wavelength region can be attributed to the absorption of the second harmonic signal by the PAH/PB film. This absorption of nonlinear molecule is due mainly to their electronic excitation, and it is generally a trade-off between short wavelength in which the molecules are transparent and the magnitude of $\chi^{(2)}$. There are extensive studies on molecular design and synthesis for second–order nonlinear chromophores that can simultaneously provide large nonlinear coefficient and exhibit low optical absorption at the desired wavelength [33].

The nonlinear fibers studies in this section are not phase matched for SHG, which limits their nonlinear conversion efficiency. In the following sections (i.e., section 4 and 5), we discuss our work on achieving phase-matching or quasi-phase matching in order to enhance SHG efficiency. Several fabrication techniques in literature can produce such a periodic structure of nonlinear film on a taper surface, e.g., laser ablation on the film surface using phase mask [34], direct electron-beam patterning [35], and photochemical patterning [36]. Furthermore, intermodal phase matching can be accomplished by adjusting taper radius down to submicron scale [37]. A more detailed study of these two possibilities is discussed below.

4. Results on Intermodal Phase Matching

As discussed in previous paragraph, it is possible to enhance SHG efficiency through intermodal phase matching. In Fig. 8, we show the effective indices (β/ω) of three different fiber modes as a function of taper radius. We assume the cladding of the fiber taper is air while the tape core is silica. We consider two processes: the conversion of fundamental pump at frequency ω and in HE_{11} mode into second harmonic signals at frequency at 2ω and in TM_{01} mode, as well as second harmonic signals in the form of HE_{21} mode. (It is worth mentioning that both processes satisfy the selection rule imposed by symmetry considerations.) The wavelength of the fundamental pump is assumed to be 1200 nm. (Correspondingly, the second harmonic is at 600 nm.) From the results in Fig. 8, it is clear that phase matching between HE_{11} and TM_{01} mode can be accomplished if taper radius is close to 0.28 μm. Similarly, phase matching between the HE_{11} and HE_{21} mode can be achieved using taper radius around 0.3 μm. Using Eq. (1), we find that under the intermodal phase-matching condition, a 100-μm-long nonlinear fiber with 40 bilayers of PB/PAH coating can achieve 10% SHG efficiency with a pump peak power of 400 W. We have investigated the feasibility of depositing multiple PB/PAH bilayers onto the nanoscale silica taper. However, intermodal phase matching requires taper diameter in the range of 500-600 nm, and we found that such a thin taper is mechanically fragile and cannot withstand repeated immersion into PAH or PB solution for electrostatic self-assembly. In this section, we restrict ourselves to the study of SHG from bare silica tapers to show the feasibility of intermodal phase matching.

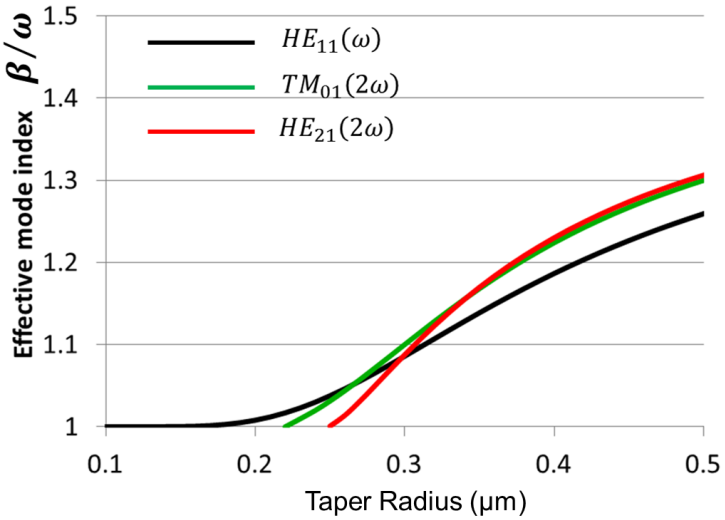

Fig. 8. Effective indices of three different fiber modes as a function of taper radius. Cladding is assumed to be air and core to be silica glass. Pump is at 1200 nm.

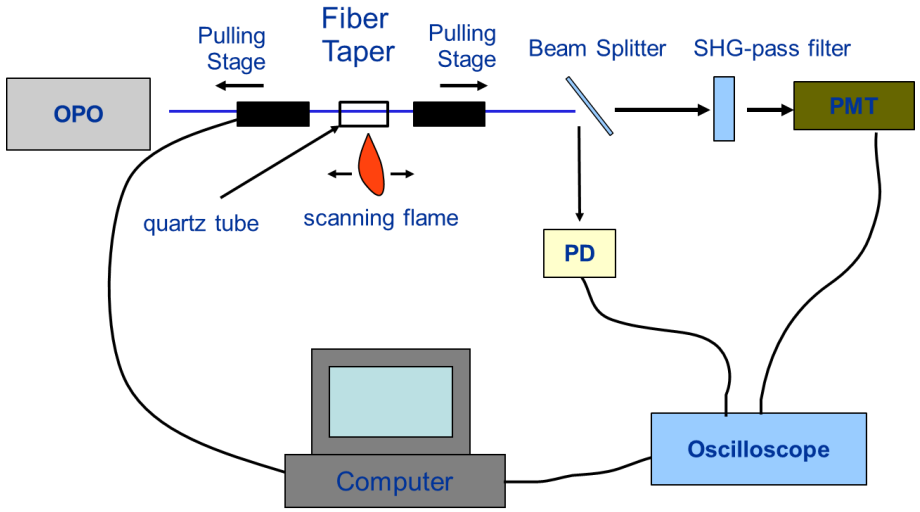

Fig. 9. The experimental system for the study of intermodal phase matching. PD: photodetector for the pump beam. PMT: photomultiplier tube for the measurement of SHG signal. The process of fiber taper pulling was controlled by computer.

Our experimental setup is illustrated in Fig. 9. Similar to the system shown in Fig. 1, the output of the OPO was coupled into a multiple mode fiber as pump beam. To achieve uniform taper profile, we scanned the heating flame across the quartz tube to achieve uniform heating of the fiber taper. As we pull the fiber taper, we used the photodiode (PD) to determine pump light intensity and used the PMT to measure SHG strength. Both pump and SHG intensity were recorded by the oscilloscope and the computer. Fig. 10 shows an example of pump light transmission and SHG signal recorded in real time during the fiber pulling process.

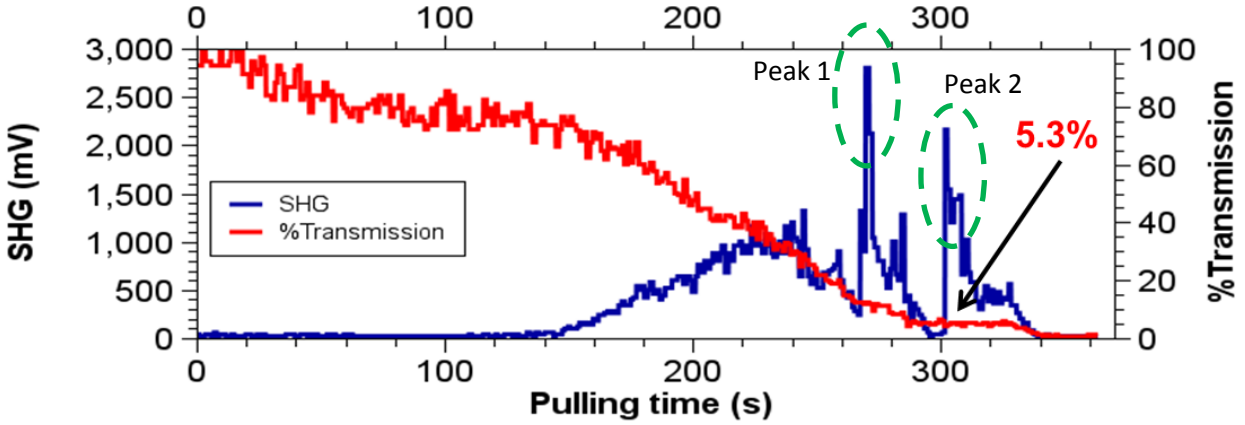

Fig. 10. The transmission of pump light (1294 nm) as well as SHG signal recorded in real time during fiber pulling. The schematic of experimental setup is shown in Fig. 9.

The solid red line in Fig. 10 represents the percentage of pump light transmitted through the fiber taper during pulling. The sold blue line represents the SHG signal, which is again recorded in real time during fiber pulling. We can identify two sets of SHG peaks. The first peak corresponds to the phase matched process of the fundamental pump in the HE_{11} mode being converted into the second harmonic in the HE_{21} mode. The second peak corresponds to the conversion of pump in the HE_{11} mode into the second harmonic in the TM_{01} mode. We note that at the 2nd peak, the transmission of the fundamental pump is only at 5.3%. One possible explanation for the low pump transmission is the optical loss caused by the transition between the multimode fiber, which possesses a large fiber core, and the small taper waist, whose radius is approximately 500 nm.

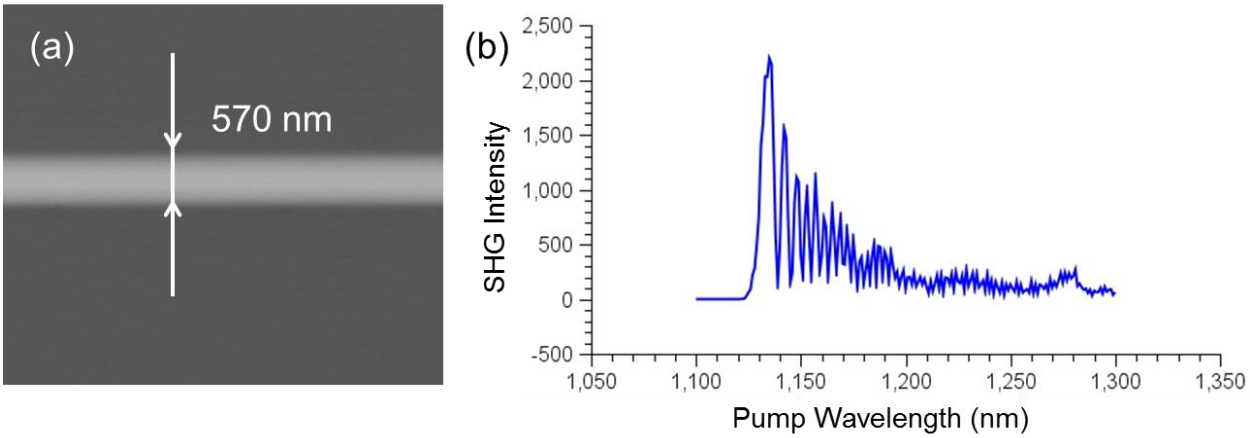

Fig. 11. (a) A SEM image of phase-matched bare taper. (b) The spectrum of SHG intensity as a function of pump wavelength. We keep pump energy at 50 nJ, which corresponds to a peak power of 5W.

With computer control, we can stop taper pulling when SHG intensity reaches either peak 1 or peak 2. Fig. 11(a) shows the SEM image of a bare silica fiber taper that can achieve intermodal phase matching with pump wavelength in the vicinity of 1200 nm. The taper waist radius, as shown in Fig. 11(a), is 570 nm, which is close to the expected value for phase matching between fundamental HE_{11} mode and the second harmonic TM_{01} mode. In Fig. 11(b), we also show the intensity of SHG signal as a function of pump wavelength. The result was obtained using the experimental system illustrated in Fig. 2. In our spectral measurements, we scanned pump wavelength while keep pump pulse energy and pump pulse peak power at 50 nJ and 5W, respectively. The data in Fig. 11(b) clearly observe the sinusoidal variations of SHG intensity, which is consistent with phase matched SHG generation. From our experimental studies, we generally find SHG energy to be 5×10^{-5} nJ per pump pulse, which corresponds to a conversion efficiency of approximately 5×10^{-6}. With our current system of fiber taper pulling, we find it difficult to significantly increase the SHG conversion efficiency beyond 10^{-4}. This is mainly due to two reasons. First, as mentioned earlier, we cannot easily deposit multiple bilayers of PB/PAH on a fiber taper with a waist radius of ~600 nm. Thus we are limited by the weak second-order nonlinearity generated at the air-silica interface. Second, with such a small fiber taper radius, it is difficult to efficiently couple pump light from the multimode fiber into the thin taper. With these constraints, we decided to try enhancing SHG efficiency by combining plasmonic enhancement with quasi-phase matching.

5. Plasmonic Enhancement and Potential for Quasi-Phase Matching

It is well know that plasmonic nanoparticles (e.g., gold or silver nanostructures) can be used to significantly enhance the strength of optical field in the vicinity of such nanoparticles. Therefore, one possible approach for enhancing SHG efficiency is to incorporate plasmonic nanoparticles onto the silica fiber taper. To test the feasibility of this approach, we have coated silica fiber tapers (5-10μm in diameter) with 30 nm gold nanoparticles and characterized optical transmission through such fiber tapers. In Fig. 12(a) (refer to next page), we show a SEM image of a fiber taper covered with such gold nanoparticles. The optical transmission spectrum through such gold-nanoparticle-coated fiber tapers are shown in Fig. 12(b). In the same figure, we also show the transmission spectrum of gold nanoparticles in aqueous solution, as represented by the solid red line. The transmission data for Au nanoparticle solution was scaled such that transmission loss at shorter wavelength (i.e., 380-450 nm) is similar to that of the fiber taper coated with gold nanoparticles. As can be seen from the figure, both set of transmission data possess almost identical peak for transmission loss through the taper. Consequently, it is

reasonable to expect that the fiber taper coated with plasmonic nanoparticles should exhibit near field enhancement.

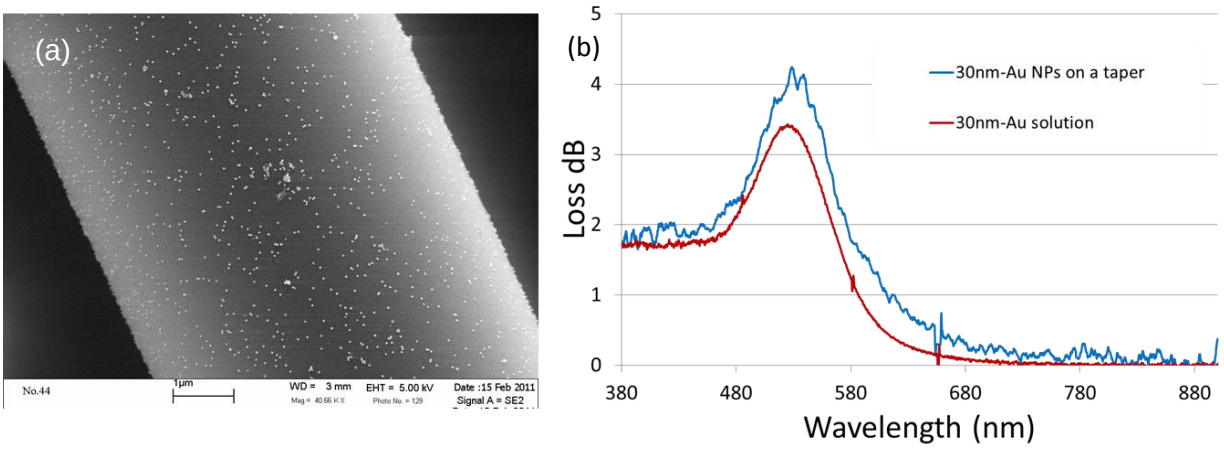

Fig. 12. (a) SEM image of a fiber taper coated with gold nanoparticles. The diameter of the gold nanoparticle is 30 nm. (b) Optical transmission through the fiber taper covered with gold nanoparticles (represented by the blue line). The red line corresponds to transmission loss through the gold nanoparticle solution, which is normalized with respect to the fiber transmission data in the wavelength range of 380 nm to 450 nm.

For second harmonic generation, the 30 nm gold nanoparticles shown in Fig. 12(a) are not entirely appropriate. This is mainly due to the fact that the plasmonic resonance is located around 550 nm. Therefore, if we were to utilize pump light at the peak of plasmonic resonance, the second harmonic wavelength will be in the range of 277 nm. However, at this wavelength, silica glass is highly absorptive. Therefore, for fiber-based SHG, we select to use gold nanorods that exhibit plasmonic resonance in the near infrared wavelength. We purchased such nanorods, and their TEM image and plasmonic resonance is shown in Fig. 13. We have utilized these nanorods to study plasmon-enhanced SHG.

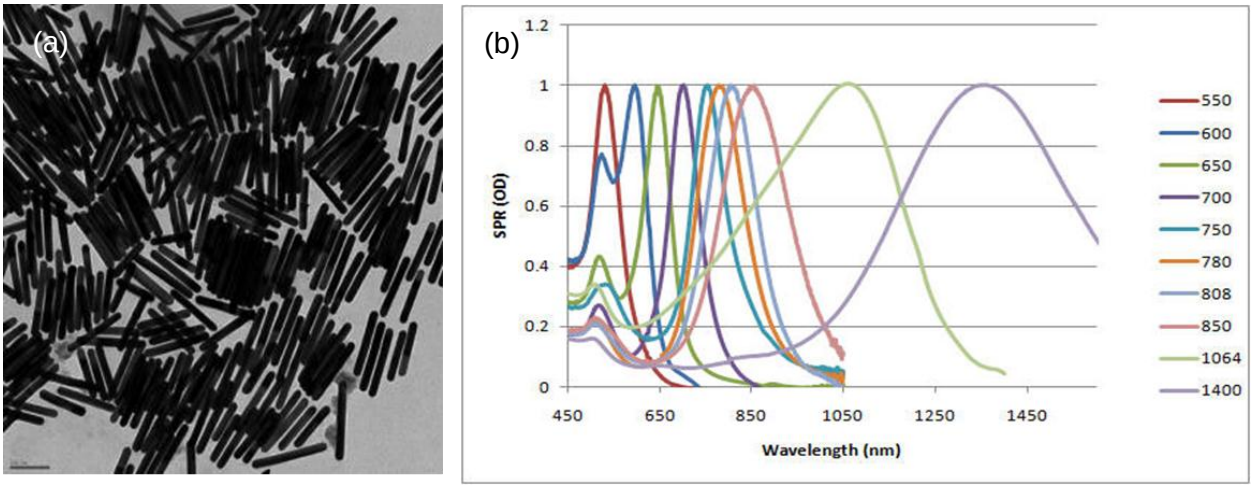

Fig. 13.(a) A TEM image of gold nanorods. (b) The plasmonic resonance of nanorods with different morphologies. We selected nanorods with resonance peak around 1400 nm.

To investigate plasmon enhanced SHG, we coat the fiber taper with 3 bilayers of PCBS and PAH. Then, we use the same self-assembly technique to cover such a nonlinear fiber taper with gold nanorods. In Fig. 14(a), we show a SEM image of such a nanorod-covered fiber taper. And

by using the same SHG measurement system shown in Fig. 2, we can obtain the intensity of SHG generation as a function of pump wavelength.

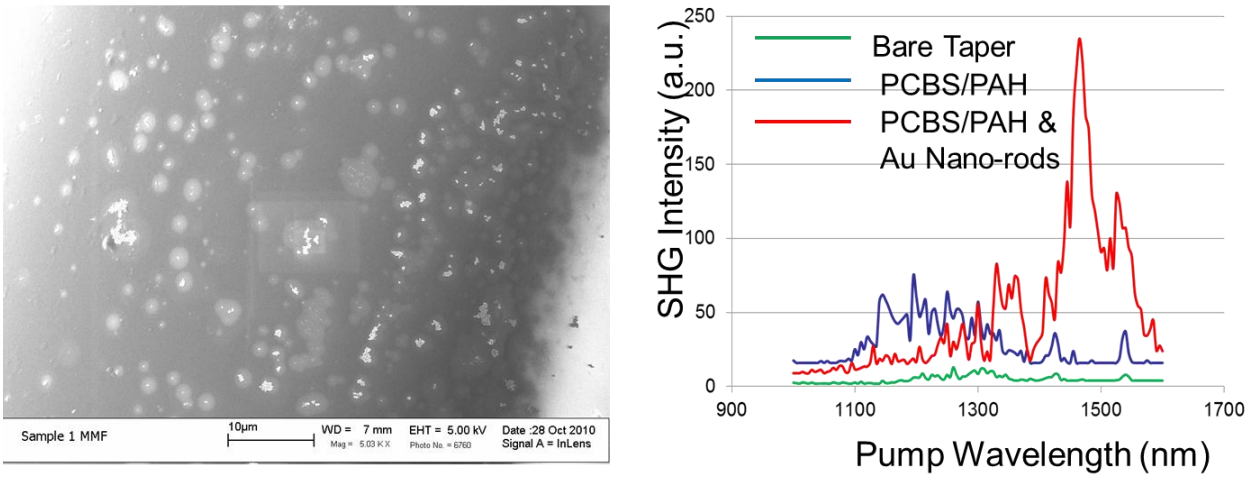

Fig. 14. (a) SEM image of a nonlinear fiber taper covered with gold nanorods. The nonlinear taper consists of a silica taper and 3 bilayers of PCBS/PAH polymers. (b) The intensity of SHG as a function of pump wavelength. The green line corresponds to the background generated by a bare fiber taper. The blue line corresponds to those generated by the nonlinear taper, i.e., a silica taper covered with 3 bilayers of PCBS/PAH. The red line corresponds to the same nonlinear taper covered with gold nanorods shown in (a). The pump pulse energy used in our experiments is 2 μJ.

In Fig. 14(b), we show SHG intensity generated by a bare taper, a nonlinear taper covered with 3 bilayers of PCBS and PAH, and the same nonlinear taper covered with gold nanorods. We clearly observed significant plasmon enhancement in the vicinity of 1500 nm. However, since nanoparticle deposition is random in nature, the overall second harmonic field generated by the taper shown in Fig. 14 is not phase matched. We are currently developing a process that can accomplish quasi-phase matching based on plasmonic enhancement. The concept of our approach is outlined in Fig. 15.

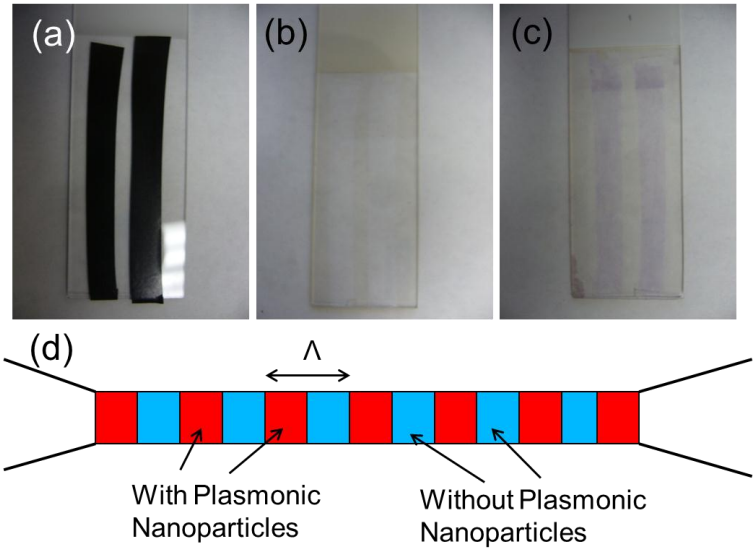

Fig. 15. (a) A glass slide covered with PAH and two stripes of tape. (b) The same slide in (a) after UV exposure and tape removal. (c) The glass slide in (b) with self-assembled nanoparticles. (d) Schematic of quasi-phase matching through plasmonic enhancement.

The basic idea behind plasmon-based quasi-phase matching is illustrated in Fig. 15(d). If we can periodically deposit plasmonic nanoparticles on nonlinear taper, we can then achieve enhanced SHG signal in the regions represented by red squares. If we arrange plasmon enhanced segments with appropriate spatial periodicity Λ, we can achieve

quasi-phase matching for the desired pump wavelength. Therefore, in order to achieve quasi-phase matching using plasmonic enhancement, we need to gain the capability of selectively depositing gold nanoparticles on localized spatial regions. We have carried out a preliminary experiment and demonstrated this feasibility. Our result is shown in Figs. 15(a) to 15(c). In particular, Fig. 15(a) shows a glass slide covered with PAH and two stripes of black tapes. Then, we placed this glass slide under a UV lamp for 2 hours to modify PAH polymer. As a result of UV exposure, the modified PAH layer can no longer attract gold nanoparticles as efficiently as unmodified PAH monolayers. To demonstrate this effect, we immerse the glass slide in Fig. 15(b) in gold nanoparticle solution. As can be seen in Fig. 15(c), in regions with unmodified PAH monolayer (i.e., under the tape and not exposed to UV light), we can self-assemble gold-nanoparticles as previous described. Yet in regions where PAH was exposed to UV light, the nanoparticles can no longer be assembled as effectively, as indicated by the lack of color change in regions no covered by the tape [refer to Fig. 15(c).] We are currently investigating the feasibility of achieving quasi-phase matching using approach presented here.

6. Microsphere Q Factors

We have coated silica microspheres with nonlinear polymers and nanoparticles and optically characterized these surface-modified silica microspheres. Our measurement system is illustrated in Fig. 16. As shown in the figure, we place a microsphere in close proximity with a tapered silica fiber with diameter around 1 μm. In order to determine the Q factor of the microsphere, we launch the output of a tunable laser into the fiber taper and measure the transmission spectrum of light as it passes through the tapered region that is coupled with the microsphere. The laser frequency is fine-tuned using external cavity modulation. From the spectrum of optical transmission through the taper region coupled with the microsphere, we can determine the cavity Q factor. It should be mentioned that in all experiments shown below, the microsphere and the taper are in direct contact with each other. Consequently, the Q factors we reported below correspond to the “loaded” Q factor, which is lower than the Q factors of a free standing microsphere.

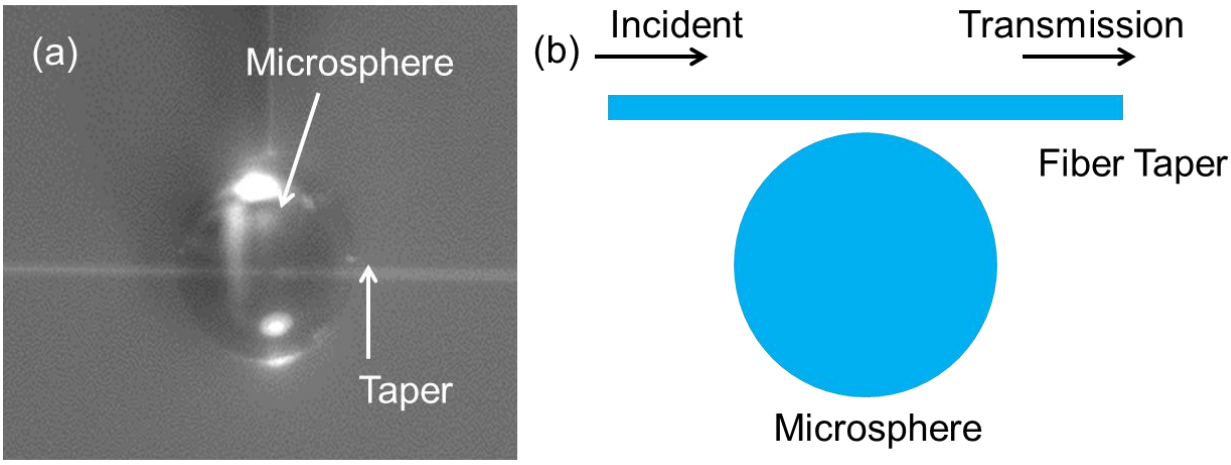

Fig. 16 (a) An image of a silica microsphere coupled with a fiber taper (approximately 1 μ in diameter). (b) Schematic of the experimental system for Q factor measurements. We measure the transmission of optical signals that pass through the fiber taper with microsphere in direct contact. The wavelength of the incident light is tuned through external cavity modulation of a tunable laser. The intensity of the transmitted signal is measured using a photodiode.

As mentioned earlier, we have coated silica microspheres with both nonlinear polymers and gold nanoparticles. The SEM images of such coated microspheres are shown in Fig. 17.

Specifically, in Fig. 17(a), we show the SEM image of a silica microsphere covered with 10 bilayers of PAH/PCBS. In Fig. 17(b), we show a silica microsphere covered with multiple 30 nm gold nanoparticles. Fig. 17(c) is a magnified image of the microsphere in (b), which clearly shows the presence of the gold nanoparticles.

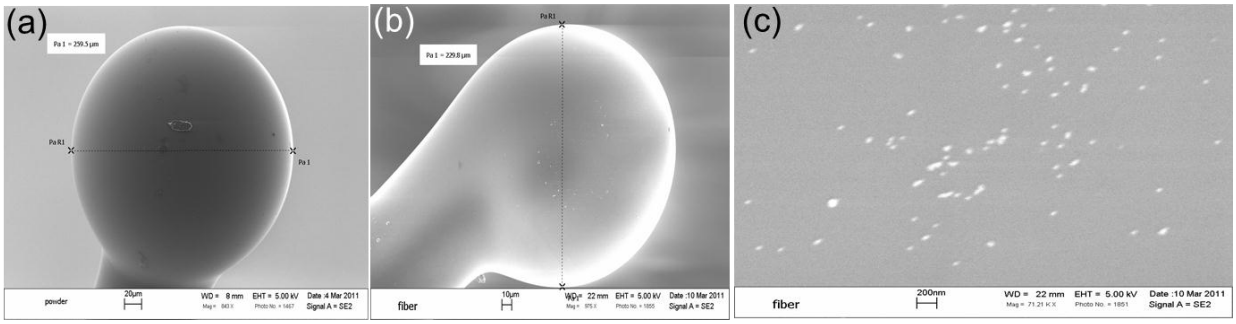

Fig. 17. (a) SEM image of a silica microsphere coated with 10 bilayers of PAH/PCBS. (b) SEM image of a silica microsphere covered with 30 nm gold nanoparticles. (c) A magnified image of the coated microsphere in (b).

After coating microspheres with nonlinear polymers and nanoparticles, we proceed to measure their transmission spectra to extract Q factors. The results are summarized below in Fig. 18.

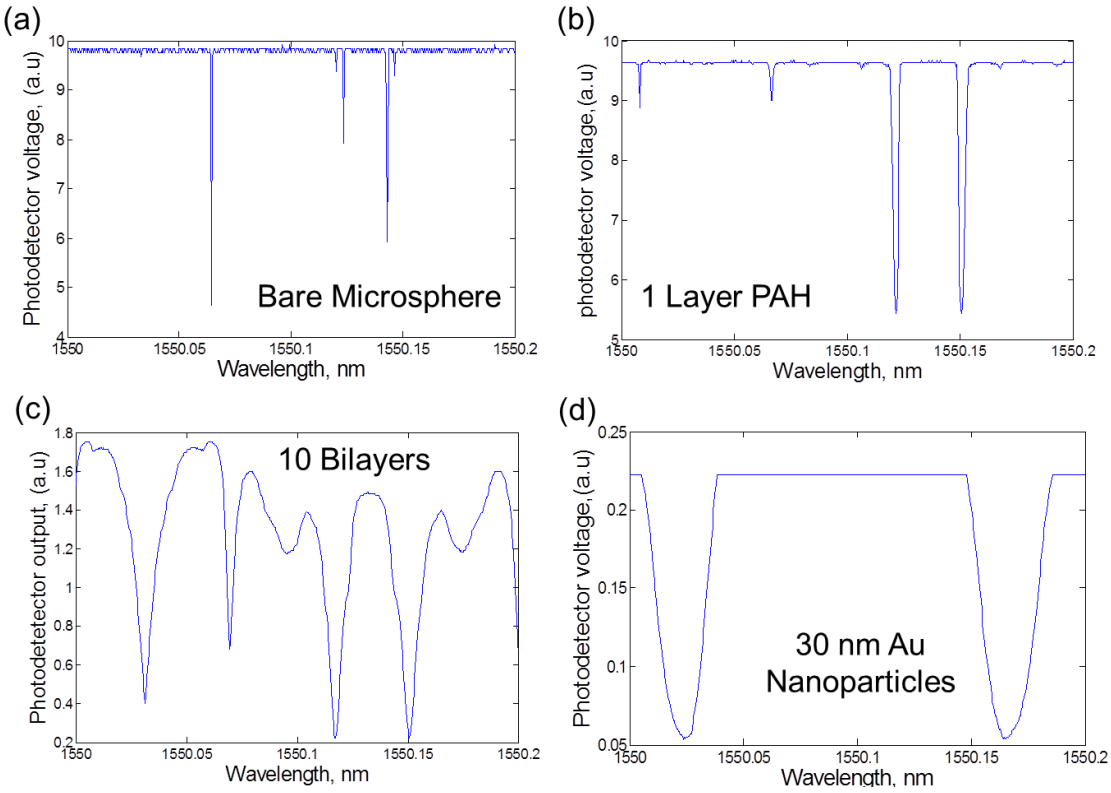

Fig. 18. The transmission spectra of: (a) a uncoated silica microsphere; (b) a microsphere covered with 1 monolayer of PAH; (c) a microsphere covered with 10 bilayers of PAH/PCBS; (d) a microsphere covered with 30 nm gold nanoparticles.

The result in Fig. 18(a) corresponds to the transmission spectrum of a bare (i.e., uncoated) silica microsphere. The sharp dips clearly indicate the existence of high Q modes. Next, we

coated a bare silica microsphere with 1 layer of PAH and again measure its transmission spectrum. As can be seen from the results in Fig. 18(b), the "dips" in the transmission spectrum becomes slightly wider, which indicates a Q factor lower than that of a bare microsphere. In Figs. 18(c) and (d), we show the transmission spectrum of a microsphere coated with 10 bilayers of PAH and PCBS [refer to Fig. 17(a)] and a microsphere covered with gold nanoparticles [refer to Figs. 17(b) and (c)].

In our experimental studies, we have measured a large number of microspheres with similar number of polymer bilayers and gold nanoparticles. The average Q factors of such microspheres are summarized in the table below. From the results shown in the table, it is clear that multiple layers of nonlinear polymers do not decrease Q factors of silica microspheres beyond 10^5. Furthermore, the results in Table 1 and Fig. 18(d) indicates that we can cover the surface of a silica microsphere with a large number of gold nanoparticles while maintaining high Q characteristics of the microsphere. We are currently studying second harmonic generation from silica microspheres covered with nonlinear polymers and plasmonic nanoparticles.

Sample	Bare	1 PAH	5 Bilayer	7 Bilayer	10 Bilayer	Au NPs
Q factor	$> 1 \times 10^7$	2.6×10^6	6.3×10^5	5.0×10^5	4.2×10^5	1.2×10^5

Table 1. The average Q factors of microspheres coated with different surface materials. All Q factor values refer to the average of results obtained using 3-5 similar samples. Samples denoted as bare and 1PAH refers to silica microspheres that are uncoated or coated with 1 monolayer of PAH. The number of bilayer refers to number of PAH/PCBS polymers. Gold nanoparticles are 30 nm in diameter.

7. Journal Publications

1) Y. Xu, A. Wang, J. R. Heflin, and Z. Liu, "Proposal and analysis of a silica fiber with large and thermodynamically stable second order nonlinearity." *Appl. Phys. Lett.*, **90** (21), Art # 211110, (2007).

2) Y. Xu, M. Han, A. Wang, Z. Liu, and J. R. Heflin, "Second order parametric processes in nonlinear silica microspheres," *Phys. Rev. Lett*., **100,** Art#163905, (2008).

3) C. Daengngam, M. C. Hofmann, Z. Liu, A. Wang, J. R. Heflin, and Y. Xu, "Demonstration of a cylindrically symmetric second-order nonlinear fiber with self-assembled organic surface layers," Accepted for publication in *Optics Express*, (2011).

4) J. Yi, C. Daengngam, J. R. Heflin, and Y. Xu, "Optical characterization of silica fiber taper with self-assembled nanoparticles," Manuscript under preparation.

5) I. Kandas, C. Daengngam, J. Yi, A. Wang, J. R. Heflin, and Y. Xu, "Characterization of high Q whispering gallery modes in silica microspheres with self-assembled polymers and nanoparticles" Manuscript under preparation.

References:

1. Agrawal, G. P. Nonlinear fiber optics. (Elsevier, Singapore, 2007)
2. B. P. Antonyuk, N. N. Novikova, N. V. Didenko, and O. A. Aktsipetrov, "All optical poling and second harmonic generation in glasses: theory and experiment," Phys. Lett. A. 287, 161-168 (2001)

3. M. K. Balakirev, V. A. Smirnov, and L. I. Vostrikova, “Photorefractive effect on all optical polling of glass,” J. Opt. A: Pure Appl. Opt. 5, S437-S443 (2003)
4. V. Tombelaine, C. Buy-Lesvigne, P. Leproux, V. Couderc, and G. Melin, “Optical poling in germanium-doped microstructured optical fiber for visible supercontinuum generation,” Opt. Lett. 33, 2011-2013 (2008)
5. R. A. Myers, N. Mukherjee, and S.R. J. Brueck, “Large second-order nonlinearity in poled fused silica fiber,” Opt. Lett. 16, 1732-1734 (1991)
6. H. An, and S. Fleming, “Second-order optical nonlinearity in thermally poled borosilicate glass,” Appl. Phys. Lett. 89, 181111(1)-181111(3) (2006)
7. A. Canagasabey, C. Corbari, Z. Zhang, P. G. Kasansky, and M. Ibsen, “Broadly tunable second-harmonic generation in periodically polled silica fibers,” Opt. Lett. 32, 1863-1865 (2007)
8. V. Pruneri, et al. “Greater than 20%-efficient frequency doubling of 1532-nm nanosecond pulses in quasi-phase-matched germanosilicate optical fiber,” Opt. Lett. 24, 208-210 (1999)
9. A. Canagasabey, et al. “High-average-power second-harmonic generation from periodically poled silica fibers,” Opt. Lett. 34, 2483-2485 (2009)
10. T. Fujiwara, M. Takahashi, and A. J. Ikushima, “Second-harmonic generation in germanosilicate glass poled with ArF laser irradiation,” Appl. Phys. Lett. 71, 1032-1034 (1997)
11. C. Corbari, P. G. Kazasky, S. A. Slattery, and N. Nikogosyan, “Ultraviolet poling of pure fused silica by high-intensity femtosecond radiation,” Appl. Phys. Lett. 86, 071106(1)-071106 (3) (2005)
12. A. Okada, K. Ishii, K. Mito, and K. Sasaki, “Phase-matched second-harmonic generation in novel corona poled glass waveguides,” Appl. Phys. Lett. 60, 2853-2855 (1992)
13. S. Horinouchi, H. Imai, G. J. Zhang, K. Mito, and K. Sasaki, “Optical quadratic nonlinearity in multilayer corona-poled glass films,” Appl. Phys. Lett. 68, 3552-3554 (1996)
14. C.-A. Tsai, et al. “Enhancement of SHG in fused SiO2 by corona poling under water, water vapor and salty environments,” J. Mar. Sci. Technol. 16, 90-102 (2008)
15. Y. Jiang, P. T. Wilson, M. Downer, C. W. White, and S. P. Withrow “Second harmonic generation from silicon nanocrystals embedded in SiO2,” Appl. Phys. Lett. 78, 766-768 (2001)
16. Y. Yamamoto, H. Nasu, T. Hashimoto, and K. Kamiya, “Second harmonic generation from thermally poled CdS microcrystal-containing glasses,” J. Non-Cryst. Solids. 281, 198-204 (2001)
17. X. Xiao, Q. Liu, G. Dong, and X. Zhao, “Second-order optical nonlinearity in Sb2S3 microcrystal doped glasses by electron beam irradiation,” Opt. Commun. 274, 456-460 (2007)
18. A. L. Moura, M. T. de Araujo, M. V. D. Vermelho, and J. S. Aitchison, “Improved stability of the induced second-order nonlinearity in soft glass by thermal poling,” J. Appl. Phys. 100, 033509(1)-033509(5) (2006)
19. T. Fujiwara, M. Takahashi, and A. J. Ikushima, “Decay behaviour of second-order nonlinearity in GeO2-SiO2 glass poled with UV-irradiation,” Electron. Lett. 33, 980-982 (1997)
20. H. Imai, et al. “Time-dependent decay of quadratic non-linearity in corona-poled silicate glass films,” J. Non-Cryst. Solids. 196, 63-66 (1996)
21. Y. Xu, A. Wang, J. R. Heflin, and Z. Liu, “Proposal and analysis of a silica fiber with large thermodynamically stable second order nonlinearity,” Appl. Phys. Lett. 90, 211110(1)-211110(3) (2007)

22. Y. Xu, M. Han, A. Wang, Z. Liu, and J. R. Heflin, “Second order parametric processes in nonlinear silica microspheres,” Phys. Rev. Lett. 100, 163905(1)-163905(4) (2008)
23. J. R. Heflin, et al. “Efficient, thermally-stable second order nonlinear response inorganic hybrid covalent/ionic self-assembled films,” Langmuir. 22, 5723-5727 (2006)
24. T. A. Brisk, and Y. W. Li, “The shape of fiber tapers,” J. Lightwave. Technol. 10, 432-438 (1992)
25. S. Xue, M. van Eijkelenborg, G. W. Barton, and P. Hambley, “Theoretical, numerical, and experimental analysis of optical fiber tapering,” J. Lightwave. Technol. 25, 1169-1176 (2007)
26. K. Van Cott, et al. “Layer-by-layer deposition and ordering of low-molecular-weight dye molecules for second order nonlinear optics,” Angew. Chem. Int. Ed. 41, 3236-3238 (2002)
27. G. Zhai, and L. Tong, “Roughness-induced radiation losses in optical micro or nanofibers,” Opt. Exp. 15, 13805-13816 (2007)
28. Y. Fujii, B. S. Kawasaki, K.O. Hill, and D. C. Johnson, “Sum-frequency light generation in optical fibers,” Opt. Lett. 5, 48-50 (1980)
29. M. A. Saifi, and M. J. Andrejco, “Second-harmonic generation in single-mode and multimode fibers,” Opt. Lett. 13, 773-775 (1988)
30. D.A. Akimov, et al. “Generation of a spectrally asymmetric third harmonic with unamplified 30-fs Cr:forsterite laser pulses in a tapered fiber,” Appl. Phys. B. 76, 515-519 (2003)
31. V. Grubsky, and J. Feinberg, “Phase-matched third-harmonic UV generation using low-order modes in a glass micro-fiber,” Opt. Commun. 274, 447-450 (2007)
32. Y. R. Shen, The principles of nonlinear optics. (John Wiley and Sons, New Jersey, 1984)
33. M. J. Cho, D. H. Choi, P. A. Sulliva, A. J. P. Akelaitis, and L. R. Dalton, “Recent progress in second-order nonlinear optical polymer and dendrimers,” Prog. Polym. Sci. 33, 1013-1058 (2008)
34. B. Brochers, J. Bekesi, P. Simon, and J. Ihlemann, “ Submicron surface patterning by laser ablation with short UV pulses using a proximity phase mask setup,” J. Appl. Phys. 107, 063106(1)-063106(4) (2010)
35. A. Rastogi, M. Y. Paik, M. Tanaka, and C. K. Ober, “ Direct patterning of intrinsically electron beam sensitive polymer brushed, “ ACS Nano. 4, 771-780 (2010)
36. F. Pan, P. Wang, K. Lee, A. Wu, N. J. Turro, and J. T. Koberstein, “Photochemical modification and patterning of polymer surface adsorption of photoactive black copolymers,” Langmuir. 21, 3605-3612 (2005)
37. U. Wiedemann et. al. “Measurement of submicrometre diameters of tapered optical fibers using harmonic generation,” Opt. Exp. 18, 7693-7704 (2010)